nature structural & molecular biology

Synergistic substrate binding determines the stoichiometry of transport of a prokaryotic H^+/Cl^- exchanger

Alessandra Picollo[1], Yanyan Xu[2], Niklaus Johner[2,3], Simon Bernèche[2] & Alessio Accardi[1,3,4]

Active exchangers dissipate the gradient of one substrate to accumulate nutrients, export xenobiotics and maintain cellular homeostasis. Mechanistic studies have suggested that two fundamental properties are shared by all exchangers: substrate binding is antagonistic, and coupling is maintained by preventing shuttling of the empty transporter. The CLC H^+/Cl^- exchangers control the homeostasis of cellular compartments in most living organisms, but their transport mechanism remains unclear. We show that substrate binding to CLC-ec1 is synergistic rather than antagonistic: chloride binding induces protonation of a crucial glutamate. The simultaneous binding of H^+ and Cl^- gives rise to a fully loaded state that is incompatible with conventional transport mechanisms. Mutations in the Cl^- transport pathway identically alter the stoichiometries of H^+/Cl^- exchange and binding. We propose that the thermodynamics of synergistic substrate binding, rather than the kinetics of conformational changes and ion binding, determine the stoichiometry of transport.

The coordinated generation and dissipation of ionic gradients by active transporters and ion channels allows cells to control and finely tune their internal ionic composition. Primary and secondary active transporters create the gradients at the expense of energy in the form of ATP hydrolysis for the former and dissipation of other electrochemical gradients for the latter. Depending on whether substrates travel together or in opposite directions, transporters are further classified as symporters or exchangers. Although active transporters differ in energy sources, substrate specificities, oligomeric organization and structure, they all function according to the archetypal paradigm of alternating access[1–7]. In this model, substrate translocation is mediated by concerted conformational rearrangements that alternatively expose the ligand-binding sites to either side of the membrane. Careful mechanistic investigations have shown that exchangers operate following ping-pong, or double-displacement, kinetics[2,8–10] (**Fig. 1a**). In these models the transporters interact with one substrate at a time, and the empty transporter does not alternate exposure of the binding sites[2,3,11]. Thus, the exchange cycle is comprised of two half-cycles during which the transporter binds and translocates each substrate (**Fig. 1a**). Simultaneous binding schemes have rarely been proposed[12,13] and have found little support, as noncanonical behaviors could also originate from allosteric substrate-binding sites on a sequential exchanger[10].

The recent surge in structural information and functional data on a number of primary and secondary active exchangers[5,14–21] has greatly refined our understanding of transport mechanisms and has provided strong support for ping-pong exchange models. One ambiguous case is the recently identified CLC family of H^+/Cl^- exchangers[22–27], for which the applicability of a ping-pong alternating access scheme has been questioned[22,28,29]. In these transporters, substrate movement takes place along two partially congruent translocation pathways[28,30]. This organization is completely different from that found in conventional exchangers, wherein substrates take turns occupying a single pathway. It has been speculated that the existence of these two pathways might allow the CLC exchangers to function by simultaneously binding both substrates[28]. The Cl^- pathway is defined by three anionic binding sites that span the length of the membrane[14,31], but only the extremities of the H^+ pathway, Glu148 and Glu203, have been identified[22,28] (**Fig. 1b**). Crystallographic work[14,29,31] has shown that Glu148 can adopt three conformations: it can occupy the external binding site, S_{ex}, with ions bound to internal and central sites, S_{in} and S_{cen}, respectively (**Fig. 1b**); when protonated, its side chain can move outside of the pathway, with all three sites occupied by Cl^- ions (**Fig. 1c**); and it can adopt a conformation in which the Glu148 side chain occupies S_{cen}, and Cl^- ions are found in S_{in} and S_{ex} (**Fig. 1d**). Furthermore, the Cl^- pathway in the known CLC structures is not completely occluded at the intracellular side[14,29], leading to the proposal that the exchange stoichiometry of two Cl^- ions for one H^+ arises from the kinetics of Cl^- unbinding rather than from a conformational change[29]. In contrast, some functional characteristics of the CLC exchangers could be described using classical schemes[32], suggesting that their transport mechanism is more conventional. Overall, the mechanism of substrate coupling and transport for these transporters remains unclear.

Recent studies have shown that the strict coupling between Cl^- and H^+ is essential to allow these proteins to regulate endosomal and lysosomal homeostasis *in vivo*: pathologies seen in mice in which a CLC transporter is replaced with a mutant mediating H^+-uncoupled Cl^- fluxes are the same as those seen in CLC transporter

[1]Department of Anesthesiology, Weill Cornell Medical College, New York, New York, USA. [2]Swiss Institute of Bioinformatics, Biozentrum, University of Basel, Basel, Switzerland. [3]Department of Physiology and Biophysics, Weill Cornell Medical College, New York, New York, USA. [4]Department of Biochemistry, Weill Cornell Medical College, New York, New York, USA. Correspondence should be addressed to A.A. (ala2022@med.cornell.edu) or S.B. (simon.berneche@unibas.ch).

Received 19 September 2011; accepted 8 March 2012; published online 8 April 2012; doi:10.1038/nsmb.2277

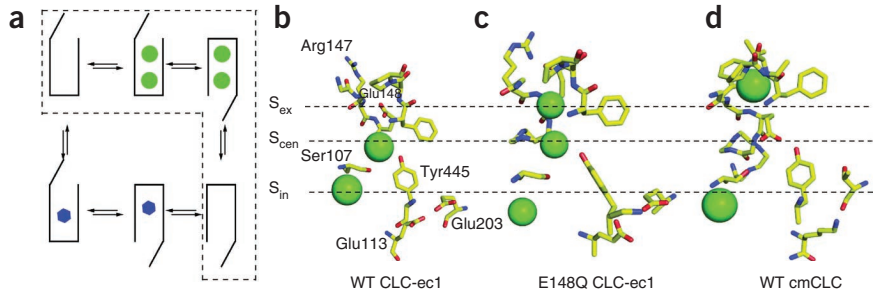

Figure 1 Alternating-access transport. (**a**) Schematic representation of a canonical alternating-access scheme for a 1:2 H^+/Cl^- exchanger. Cl^-, green circles; H^+, blue hexagons. The dashed line highlights the Cl^- half-cycle. (**b**–**d**) Close-up views of the ion-binding regions of CLC-family exchangers: WT CLC-ec1 (**b**), the E148Q mutant of CLC-ec1 (**c**) and WT cmCLC (**d**). Cl^- ions are shown as green spheres. Key residues are labeled. For WT cmCLC, the residues equivalent to those labeled in **b** are displayed: Arg147 equates to Trp209, Glu113 to Lys171 and Glu203 to Thr269. PDB accession codes: WT CLC-ec1, 1OTS[31]; E148Q CLC-ec1, 1OTU[31]; WT cmCLC, 3ORG[29].

knockout mice[33]. Therefore, understanding the molecular basis for substrate coupling in the CLC exchangers is essential for understanding their transport mechanism and their physiological role.

Here we investigate the coupling mechanism of the CLC exchangers using isothermal titration calorimetry (ITC) and free energy calculations. We asked whether binding of Cl^- and H^+ to CLC-ec1 is linked, and, if so, whether it is antagonistic (as required by canonical double-displacement mechanisms). We find that substrate binding to CLC-ec1 is synergistic (Cl^- binding to the transport pathway facilitates protonation of a crucial glutamate residue), sequential (Cl^- binds first, followed by H^+) and simultaneous (both substrates can bind to the protein at the same time).

RESULTS

We used ITC to determine whether Cl^- binding to CLC-ec1 is linked to the exchange of a H^+. The total enthalpy measured during an ITC experiment, ΔH_{tot}, results from several protein-specific reactions (Cl^- binding, conformational changes and protonation or deprotonation of the protein) and the ionization of the buffer donating or accepting the protons exchanged by the protein[34–36]. Therefore, ΔH_{tot} can be written as:

$$\Delta H_{tot} = \Delta H_{prot} + N\Delta H_{buff} \qquad (1)$$

where ΔH_{prot} denotes the sum of the enthalpies of the protein-specific reactions, ΔH_{buff} is the enthalpy of ionization of the buffer and N is the number of protons exchanged between protein and buffer per Cl^- binding event. ΔH_{buff} is a buffer-specific quantity and can be directly measured in the absence of protein (**Supplementary Table 1**). Therefore, the slope of the linear relationship between ΔH_{tot} and ΔH_{buff} is the stoichiometry of coupled Cl^- and H^+ binding. If substrate binding to CLC-ec1 is not coupled, then ΔH_{tot} should not vary when measured in buffers with different ΔH_{buff} values, so that $N = 0$. Conversely, a direct coupling between substrate binding would be revealed by a variable ΔH_{tot} value. A negative slope would indicate that Cl^- binding induces unbinding of a proton from CLC-ec1 (antagonistic binding), whereas a positive slope would indicate that Cl^- binding promotes protonation of CLC-ec1 (synergistic binding).

Cl^- binding induces protonation of CLC-ec1

We measured Cl^- binding to wild-type CLC-ec1 in three buffers—Tris, HEPES and phosphate buffer—whose ΔH_{buff} values range from 0.8 to 7.4 kcal mol^{-1} (**Supplementary Table 1**) and fit the liberated heats with single-site binding isotherms[37]. Chloride binds with comparable affinities in all three buffers (**Table 1**), indicating that the buffer molecules do not interact with the binding sites. We found that ΔH_{tot} increases monotonically with the ionization enthalpy of the buffers: the enthalpy in phosphate buffer (-8.3 ± 0.2 kcal mol^{-1}), is larger than that in HEPES (-7.5 ± 0.2 kcal mol^{-1}), which is larger than that in Tris (-5.1 ± 0.3 kcal mol^{-1}; **Fig. 2** and **Table 1**). Thus, chloride binding to the transport pathway induces protonation of CLC-ec1, indicating that substrate binding is synergistic and that, at equilibrium, H^+ and Cl^- simultaneously bind to the protein. The stoichiometry of this coupling is derived by fitting ΔH_{tot} to equation (1) and is $N = 0.5 \pm 0.1$. Thus, for roughly every two chloride binding events, one proton associates to CLC-ec1.

The identity of the stoichiometries of transport and binding suggests that these linked binding events are part of the exchange cycle. An alternative explanation could be that the absorbed heat reflects protonation of one or more residues outside the anion pathway in a serendipitous coincidence of the stoichiometries. To test whether this is the case, we introduced mutations that alter the stoichiometry of transport and asked how they affect the stoichiometry of binding. We mutated three residues: Glu148, Glu203 and Tyr445, which line the Cl^- pathway (Glu148 and Tyr445) or the H^+ pathway (Glu148 and Glu203) and are involved in H^+ coupling[22,28,38]. Mutating either glutamate residue to alanine or glutamine completely abolishes

Table 1 Thermodynamic parameters for Cl^- binding to WT and mutant CLC-ec1 in different buffers

	Buffer	n	ΔH_{tot} (kcal mol^{-1})	$T\Delta S$ (kcal mol^{-1})	ΔG (kcal mol^{-1})	K_d (μM)	No. exp.
WT	Tris	1	−5.1 ± 0.3	−0.9 ± 0.2	−4.3 ± 0.1	780 ± 60	9
	HEPES	1	−7.5 ± 0.2	−3.2 ± 0.2	−4.3 ± 0.1	640 ± 40	8
	Phosphate	1	−8.3 ± 0.2	−3.9 ± 0.2	−4.4 ± 0.1	680 ± 80	7
E148A	Tris	1.8 ± 0.1	−12.0 ± 1.0	−0.1 ± 0.5	−6.6 ± 0.1	15 ± 1	5
	HEPES	1.98 ± 0.03	−12.9 ± 0.5	−0.1 ± 0.3	−6.7 ± 0.1	13 ± 1	3
	Phosphate	1.5 ± 0.1	−13.5 ± 1.3	−2.3 ± 0.5	−6.6 ± 0.1	14 ± 2	5
E203Q	Tris	1	−2.1 ± 0.1	−0.8 ± 0.1	−2.9 ± 0.1	7300 ± 760	3
	HEPES	1	−3.7 ± 0.6	−0.7 ± 0.6	−3.0 ± 0.1	5800 ± 220	3
	Phosphate	1	−5.1 ± 0.3	−2.1 ± 0.3	−3.1 ± 0.1	6300 ± 340	4
Y445L	Tris	1	−3.9 ± 0.2	−0.75 ± 0.2	−3.2 ± 0.1	4600 ± 400	4
	HEPES	1	−4.6 ± 0.3	−1.3 ± 0.3	−3.3 ± 0.1	4100 ± 270	4
	Phosphate	1	−4.7 ± 0.1	−1.4 ± 0.1	−3.4 ± 0.1	4100 ± 50	4

K_d and ΔH were obtained from a fit to a binding isotherm, and free energy difference (ΔG) and entropy ($T\Delta S$) were calculated from $\Delta G = RT \ln K_d$ and $T\Delta S = \Delta H - \Delta G$, where R is the molar gas constant and T the temperature. We fixed the number of Cl^- binding sites to $n = 1$ for WT, E203Q and Y445L. We let n vary freely for the E148A mutant, as for this mutant we could achieve experimental conditions in which n can be independently determined. In all cases, ΔH_{tot} represents the total enthalpy generated during the binding reaction rather than the enthalpy for each independent binding site. For WT, Glu203 and Y445L ΔH and ΔH_{tot} coincide, whereas for the E148A mutant $\Delta H_{tot} = n\Delta H$. Values are reported as the mean ± s.e.m. of the independent experiments.

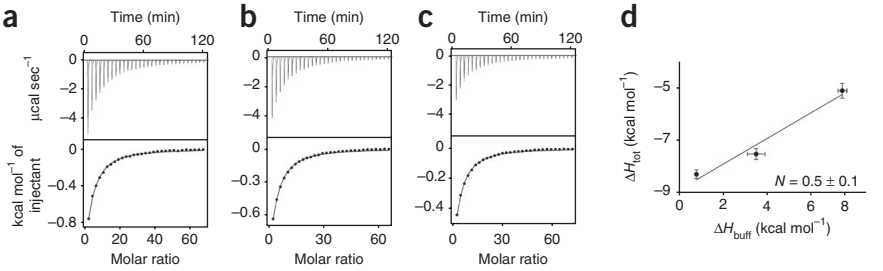

Figure 2 Synergistic binding of H^+ and Cl^- to WT CLC-ec1. (**a**–**c**) Top panels: heat liberated when a 25 mM KCl solution is injected into the experimental chamber containing WT CLC-e1 and phosphate buffer (**a**), HEPES (**b**) or Tris (**c**). Each downward deflection corresponds to one injection. Bottom panels: the area underneath each deflection is integrated and represents the total heat exchanged (circles). Black lines are the best fits to a single-site binding isotherm. Number of experiments and averaged thermodynamic parameters are reported in **Table 1**. (**d**) Plot of the total enthalpy, ΔH_{tot}, of Cl^- binding as a function of the enthalpy of buffer ionization, ΔH_{buff}. Circles, experimental data; solid line, fit to equation (1) with $\Delta H_{prot} = -8.9 \pm 0.4$ kcal mol^{-1} and $N = 0.5 \pm 0.1$. The errors for the experimental points are the s.e.m., and those on ΔH_{prot} and N represent the uncertainty of fit.

H^+ transport[22,28], and the Y445L mutation degrades Cl^--to-H^+ transport stoichiometry from 2:1 to ~6:1 (ref. 38). Chloride binding to the purified E148A transporter is nearly iso-enthalpic (**Fig. 3** and **Table 1**): the total enthalpies of Cl^- binding in the different buffers are indistinguishable (ΔH_{tot} (phosphate buffer) = -13.5 ± 1.3 kcal mol^{-1}; ΔH_{tot} (HEPES) = -12.9 ± 0.5 kcal mol^{-1}; ΔH_{tot} (Tris) = -12.0 ± 1.0 kcal mol^{-1}; $P > 0.4$). Therefore, the E148A mutation completely abolishes coupling between H^+ and Cl^- both in the transport cycle and in binding. The Y445L mutation also influences both processes to a similar extent: Cl^- binding still promotes protonation, but the stoichiometry is drastically reduced, to $N = 0.12 \pm 0.07$ (**Fig. 4** and **Table 1**), a value within experimental error of the stoichiometry of transport of ~0.17 seen in this mutant[38]. Thus, two mutations in the anion transport pathway have parallel effects on the ability of the protein to couple Cl^- and H^+ transport and binding. In contrast, the E203Q mutation leaves the stoichiometry of binding nearly unaltered, at $N = 0.43 \pm 0.05$ (**Fig. 5** and **Table 1**), but it eliminates coupled exchange. Therefore, our data suggest that binding of Cl^- induces protonation of a single residue within the transport pathway, Glu148, as mutating this residue is sufficient to abolish coupled binding and transport. In contrast, protonation of Glu203, another essential step in the transport cycle, is independent of Cl^- binding.

The free energy of protonation of Glu148 is Cl^- dependent

How does Cl^- binding control protonation of Glu148? We used all-atom molecular dynamics simulations to calculate the protonation free energy (ΔG) of Glu148 and Glu203 considering different Cl^- occupancy states of the transport pathway (see **Supplementary Table 2** for a complete list of the calculations). When no ions are present in the pathway, Glu148 relaxes to a position close to S_{cen} (**Supplementary Fig. 1a**), where its protonation is extremely unfavorable, with a very high free energy of protonation ($\Delta G_{0Cl^-} = 17.3 \pm 4.5$ kcal mol^{-1}). We then analyzed the effect that occupancy of a single ion-binding site, either S_{ex} or S_{cen}, has on the work required to protonate Glu148. We found that when a Cl^- ion occupies S_{cen}, Glu148 stably resides in S_{ex} (**Supplementary Fig. 1b**), and its protonation free energy ΔG_{1Cl^-} is reduced by ~16 kcal mol^{-1} to 1.1 ± 0.7 kcal mol^{-1} (**Fig. 6a**). In contrast, occupancy of S_{ex} by a Cl^- ion has a much smaller effect on the energy required to protonate Glu148 positioned in S_{cen} (**Fig. 6a** and **Supplementary Fig. 1c**), so that this process remains unfavorable, with an associated free energy difference $\Delta G_{1Cl^-} = 9.2 \pm 1.4$ kcal mol^{-1}. Finally, when we placed two Cl^- ions in the transport pathway, at S_{cen} and S_{ex}, protonation of the Glu148 side chain, located outside the pathway (**Fig. 6a** and **Supplementary Fig. 1d**), became strongly favored, with $\Delta G_{2Cl^-} = -9.4 \pm 3.2$ kcal mol^{-1}.

In contrast to these results, our calculations suggest that the ΔG of protonation of Glu203 is independent from the Cl^- occupancy of the transport pathway (**Fig. 6b**). It is worth emphasizing that several assumptions, such as the protonation state of individual residues of CLC-ec1, affect the absolute values of the calculated ΔG values. For example, the ΔG of protonation of Glu203 is extremely sensitive to the protonation state of Glu113 (**Supplementary Table 2** and discussion in Online Methods). Therefore, the absolute values of the reported free energies of protonation in the different configurations are difficult to interpret, and their translation into pK_a values would be inappropriate. However, the effects of Cl^- binding on the free energy of protonation for Glu148 and Glu203 are unaffected by these choices: protonation of Glu148 is unfavorable with no Cl^- ions bound and favored by double occupancy of the pathway, regardless of whether Glu113, Glu203 or both are protonated or not (**Supplementary Table 2**). Similarly, the work needed to protonate Glu203 is independent of the number of Cl^- ions bound for all protonation states of Glu113, Glu202 and Glu148 (**Supplementary Table 2**).

Our simulations suggest key roles for two factors in regulating the work required to protonate Glu148: the hydrogen bond network formed by Glu148 with the protein, and the electrostatic interactions between Glu148 and the Cl^- ions. When no Cl^- ions are bound to the pathway, the side chain of Glu148 relaxes to a position close to the

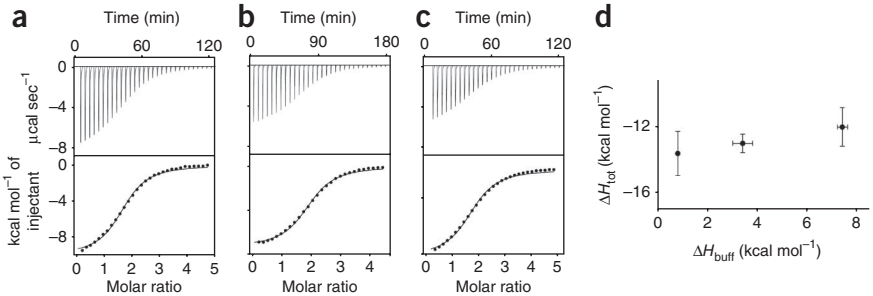

Figure 3 The E148A mutant uncouples Cl^- and H^+ binding. (**a**–**c**) Panels as in **Figure 2**, with E148A mutant and a 5-mM KCl solution injected into the experimental chamber. In these fits N was kept as a free parameter rather than fixed. (Number of experiments and averaged thermodynamic parameters are reported in **Table 1**.) (**d**) Plot of the total enthalpy, ΔH_{tot}, of Cl^- binding as a function of the enthalpy of buffer ionization, ΔH_{buff}. Circles, experimental data. The data points are indistinguishable, $P > 0.4$, Student's t-test; the errors for the experimental points are the s.e.m.

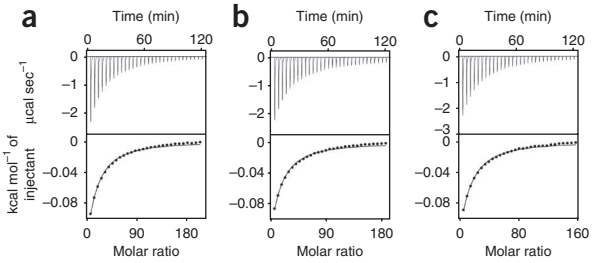

Figure 4 Cl^--coupled H^+ binding to the Y445L mutant. (**a**–**c**) Panels as in **Figure 2** with Y445L mutant and 75–100 mM KCl titrated into the experimental chamber. (Number of experiments and averaged thermodynamic parameters are reported in **Table 1**.) (**d**) Plot of the total enthalpy, ΔH_{tot}, of Cl^- binding as a function of the enthalpy of buffer ionization, ΔH_{buff}. Circles, experimental data; solid line, fit to equation (1) with $\Delta H_{prot} = -4.9 \pm 0.3$ kcal mol^{-1} and $N = 0.12 \pm 0.07$. The errors for the experimental points are the s.e.m. and those for ΔH_{prot} and N represent the uncertainty of fit.

central binding site (**Fig. 6c** and **Supplementary Fig. 1a**), similar to the conformation observed in the structure of cmCLC[29] (**Fig. 1d**), where it is stabilized by a network of hydrogen bonds with proton donor groups from different residues (the backbone of Glu148, Gly149, Ile356 and Phe357 and the hydroxyl group of Tyr445). This conformation limits the access of water molecules to the carboxylate group of Glu148, further stabilizing the unprotonated state of Glu148. This coordination network is only slightly affected by the presence of a Cl^- ion bound to S_{ex}, so that protonation of Glu148 in S_{cen} remains energetically unfavorable (**Fig. 6d**). An ion in the central site stabilizes the Glu148 side chain in the external site, where it still interacts with protein residues (Arg147, Glu148 and Ala358) but becomes more accessible to water molecules, so that its carboxylate group becomes relatively well solvated (**Fig. 6e**). The increased hydration, together with the electrostatic influence of the ion bound to the central site, drastically lowers the free energy of protonation, by ~17 kcal mol^{-1}. When the pathway is occupied by two ions, the Glu148 side chain is extended toward the extracellular solution and interacts with the side chain of Arg147 and water molecules (**Fig. 6f**). The proximity of two negatively charged Cl^- ions, together with the increased accessibility of water molecules to Glu148, greatly favors protonation, as reflected by the drastically lowered ΔG (**Fig. 6a** and **Supplementary Table 2**). Once protonated, the side chain of Glu148 can either remain solvated or form a hydrogen bond with the Cl^- ion in the external binding site (**Fig. 6f**).

Dependence on pH of Cl^- uptake in wild-type and mutant CLC-ec1

The above results suggest that Cl^- binding modulates the protonation of Glu148 by directly perturbing its pK_a. This would predict that there should be a correlation between degraded coupling of binding and altered pK_a of transport. We tested this hypothesis by measuring the pH dependence of transport mediated by wild-type (WT) or mutant CLC-ec1. We used the $^{36}Cl^-$ uptake assay rather than the Cl^- efflux assay[39], because at pH >5.5, protein-free liposomes show substantial leak to Cl^- after valinomycin and carbonylcyanide *p*-trifluoromethoxyphenylhydrazone are added to initiate efflux (**Supplementary Fig. 2**). The rate of $^{36}Cl^-$ uptake is a direct measure of the rate of the half-cycle, rather than the full turnover, of an exchanger (**Fig. 1a**). The rate of uptake mediated by the WT protein is strongly enhanced at acidic pH[40,41] (**Fig. 7a**), with an apparent pK_a of 6.2 ± 0.1 (**Fig. 7**). Uptake mediated by the E148A mutant is pH independent[41] (**Fig. 7b**), whereas the other two mutants tested, E203Q and Y445L, maintain robust pH dependencies[28] (**Fig. 7c**,**d**). Consistent with our hypothesis, the apparent pK_a of uptake mediated by the E203Q mutant, 6.2 ± 0.5, is very close to that of the WT, whereas that of the Y445L mutant is severely shifted, to 4.7 ± 0.1 (**Fig. 7e**,**f**). The strong correlation between disruption of the equilibrium coupling stoichiometry and the apparent pK_a of the half-cycle of CLC-ec1 is consistent with our hypothesis that Cl^- binding modulates the protonation probability of Glu148 by shifting its pK_a.

Cl^- binding to CLC-ec1 is pH independent

Our results suggest that Cl^- binding and protonation of the Glu148 side chain are energetically linked. However, the high ΔG for protonation of Glu148 in the absence of Cl^- (**Fig. 6a**) suggests that, at physiological concentrations, protons might not be able to drive Cl^- binding. To test this hypothesis, we measured Cl^- binding in a wide pH range (4.5–7.5) and found that a thousand-fold increase in H^+ concentration is unable to promote Cl^- binding (**Supplementary Fig. 3**). This result is consistent with the hypothesis that a high free energy barrier prevents protonation of Glu148 in the empty pathway so that Cl^- binding is not driven by H^+. Thus, substrate association to CLC-ec1 is strictly sequential (at least at physiological pH): Cl^- binding is followed by protonation of Glu148.

DISCUSSION

We used a combination of ITC measurements and free energy calculations to investigate the mechanism of coupled substrate binding and transport in CLC-ec1, a H^+/Cl^- exchanger. We found that binding of the two substrates to the WT protein is energetically linked, such that occupancy of the Cl^- transport pathway determines the protonation state of Glu148, which is the extracellular gating glutamate. In contrast, the protonation state of the intracellular proton acceptor, Glu203, is unaffected by Cl^- binding to the pathway. Our data show that with no ions bound, protonation of Glu148 is extremely unfavorable, whereas binding of one or two Cl^- ions favors and stabilizes protonation. Our ITC measurements show that the linked binding of Cl^- and H^+ is stoichiometric: for roughly every two Cl^- binding events, there is one protonation event of Glu148. Several lines of evidence suggest that these coupled binding events are part of the transport cycle.

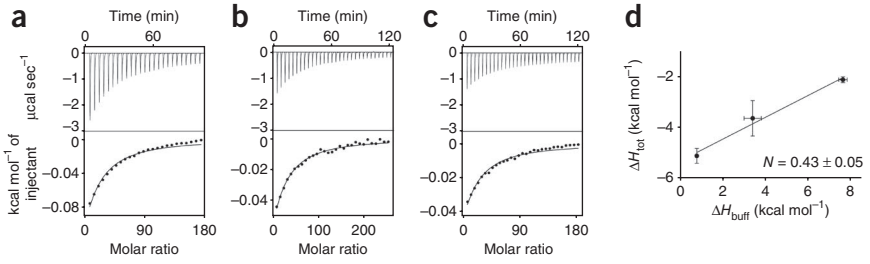

Figure 5 Cl^--coupled H^+ binding to the E203Q mutant. (**a**–**c**) Panels as in **Figure 2** with E203Q mutant and 75–100 mM KCl titrated into the experimental chamber. (Number of experiments and averaged thermodynamic parameters are reported in **Table 1**.) (**d**) Plot of the total enthalpy, ΔH_{tot}, of Cl^- binding as a function of the enthalpy of buffer ionization, ΔH_{buff}. Circles, experimental data; solid line, fit to equation (1) with $\Delta H_{prot} = -5.4 \pm 0.3$ kcal mol^{-1} and $N = 0.43 \pm 0.05$. The errors for the experimental points are the s.e.m., and those for ΔH_{prot} and N represent the uncertainty of fit.

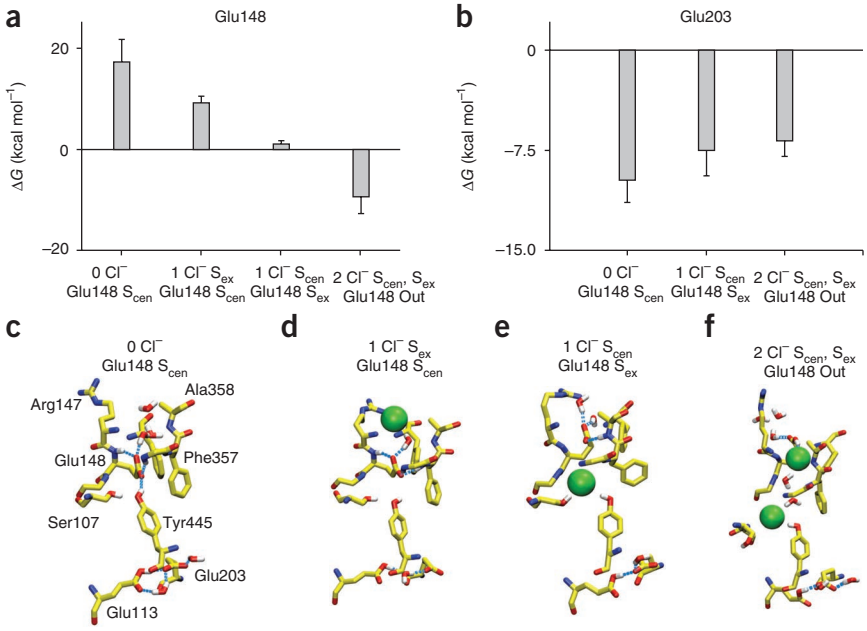

Figure 6 Modulation of the free energy of protonation of Glu148 and Glu203 by Cl^- occupancy of the anion transport pathway. (**a**,**b**) Average protonation free energy (ΔG) of residues Glu148 (**a**) and Glu203 (**b**) calculated for the different Cl^- occupancy states of the transport pathway shown in **c**–**f**. The free energy values are the average of the ΔG of protonation and deprotonation calculated with protocols A and B (see Online Methods and **Supplementary Table 2** for the complete list of calculations). The error bars represent the s.e.m. of the average. For Glu148 we considered Glu113 to be protonated, and for Glu203 we considered no other residues protonated. (**c**–**f**) Representative conformation of the ion-binding region in presence of no Cl^- ions (**c**), one Cl^- bound to S_{ex} and Glu148 in S_{cen} (**d**), one Cl^- bound to S_{cen} and Glu148 in S_{ex} (**e**) or two Cl^- (**f**) after at least 2 ns of molecular dynamics simulations. The Glu148 side chain is protonated in **f**. Cl^- ions are shown as green spheres. Only some key hydrogen atoms are shown (white sticks).

First, the stoichiometries of transport and of linked binding coincide: for every two Cl^- ions that bind to the protein and are transported, one proton binds and is exchanged (**Fig. 2** and **Supplementary Fig. 4**). Mutation of residues Glu148 and Tyr445, which directly line the Cl^- pathway, has identical effects on the stoichiometries of both transport and coupled binding (**Figs. 3** and **4** and **Supplementary Fig. 4**). In contrast, mutating Glu203, which lines only the H^+ pathway and is ~10 Å from the Cl^- pathway (**Fig. 1b**), disables H^+ transport but leaves coupled binding of Cl^- and H^+ unaltered (**Fig. 5** and **Supplementary Fig. 4**). Second, the enhancement of the rate of $^{36}Cl^-$ uptake at low pH (**Fig. 7a**) implies that during the Cl^- half-cycle (**Fig. 1a**), a H^+ also binds to CLC-ec1. Furthermore, there is a clear correlation between the effect of mutations on the binding stoichiometry (**Figs. 2**–**4** and **Supplementary Fig. 4**) and shifts of the apparent pK_a of Glu148 as measured using the $^{36}Cl^-$ uptake assay (**Fig. 7e**,**f**). Third, the protonation free energy of Glu148 is exquisitely sensitive to the number of Cl^- ions bound to the pathway: double occupancy is required to stabilize a proton bound to this residue (**Fig. 6a**). In contrast, the work required to protonate Glu203 (**Fig. 6b**) and Glu113 (**Supplementary Table 2**) is unaffected by Cl^- occupancy of the pathway. Taken together, our data suggest that in CLC-ec1, coupled transport requires the formation of a state in which both substrates are simultaneously bound to the transport pathway. This fully loaded state is incompatible with a canonical double-displacement exchange mechanism, as this paradigm requires antagonistic substrate binding. In contrast, our data show that transport mediated by CLC-ec1 entails the sequential binding of at least one Cl^- ion followed by protonation of Glu148.

On the interpretation of the stoichiometry of linked binding

The most straightforward interpretation of the 2:1 stoichiometry of linked Cl^- and H^+ binding would be that our ITC experiments report on binding to a state with two Cl^- and one H^+ bound (**Fig. 6f**). However, in our previous work[37] we described the calorimetric data for WT CLC-ec1 with a single-site binding isotherm, whereas the present interpretation requires binding of two Cl^- ions. Our earlier conclusion[37] was based on two considerations: first, the structures

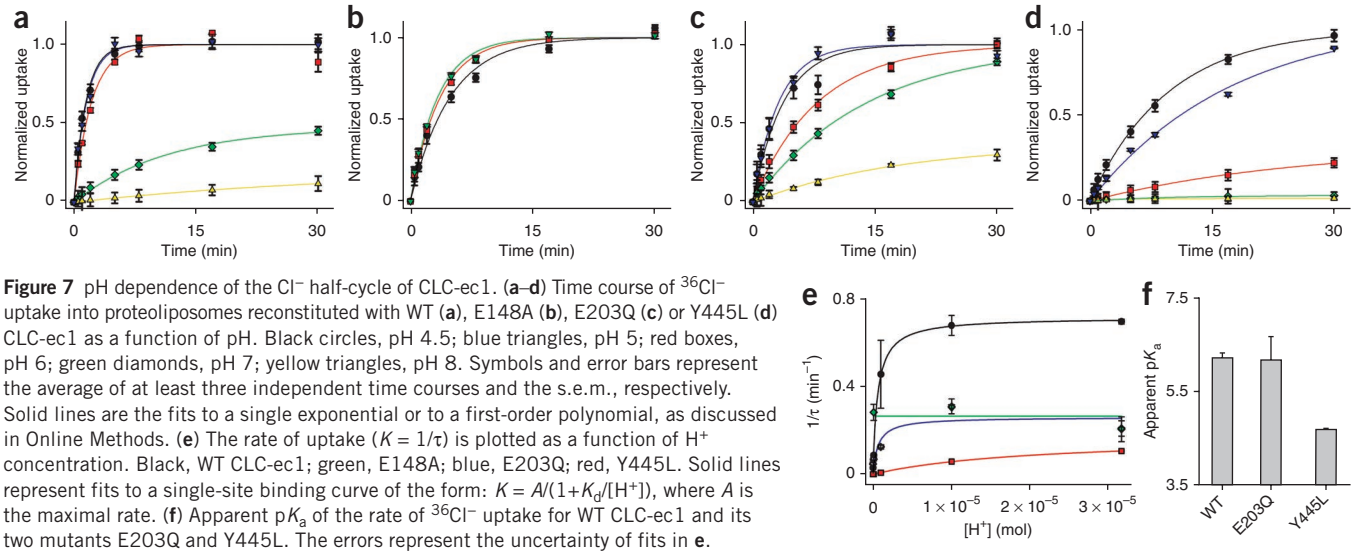

Figure 7 pH dependence of the Cl^- half-cycle of CLC-ec1. (**a**–**d**) Time course of $^{36}Cl^-$ uptake into proteoliposomes reconstituted with WT (**a**), E148A (**b**), E203Q (**c**) or Y445L (**d**) CLC-ec1 as a function of pH. Black circles, pH 4.5; blue triangles, pH 5; red boxes, pH 6; green diamonds, pH 7; yellow triangles, pH 8. Symbols and error bars represent the average of at least three independent time courses and the s.e.m., respectively. Solid lines are the fits to a single exponential or to a first-order polynomial, as discussed in Online Methods. (**e**) The rate of uptake ($K = 1/\tau$) is plotted as a function of H^+ concentration. Black, WT CLC-ec1; green, E148A; blue, E203Q; red, Y445L. Solid lines represent fits to a single-site binding curve of the form: $K = A/(1+K_d/[H^+])$, where A is the maximal rate. (**f**) Apparent pK_a of the rate of $^{36}Cl^-$ uptake for WT CLC-ec1 and its two mutants E203Q and Y445L. The errors represent the uncertainty of fits in **e**.

available at the time showed that a deprotonated Glu148 occupies S_{ex} (**Fig. 1b**) and that upon protonation, its side chain moves out of the pathway[31] (**Fig. 1c**); second, mutations that selectively disrupt binding to the central site[38,42] also weaken the binding affinity measured with ITC and equilibrium dialysis[37]. Two new observations, however, suggest that other configurations could contribute to the heat absorbed during our ITC experiments. First, the recently published structure of cmCLC[29] revealed a state in which the gating glutamate (Glu210 in cmCLC) occupies S_{cen}, and a Cl^- ion is bound to S_{ex} (**Fig. 1d**). The similar affinity of Cl^- for the central and external sites[37,43] further complicates the distinction between S_{ex} and S_{cen}. Thus the binding data could be a result of Cl^- binding to CLC-ec1 in a combination of these two states with a single Cl^- ion bound (**Fig. 6d**,**e**). Second, as we show here, Cl^- binding promotes protonation of Glu148. When this happens, binding of the Glu148 side chain to the pathway is destabilized, favoring a conformation similar to that of the E148Q mutant[31] (**Fig. 1c**). Therefore, we propose that at least part of the heat detected in our ITC experiments could arise from a state with two Cl^- and one H^+ bound. The main objection to this hypothesis is that Cl^- binds to the E148A and E148Q mutants with a K_d of ~15 μM, rather than the K_d of ~700 μM seen for the WT protein[37] (**Table 1**). However, these mutants are imperfect mimics of the protonated state of the gating glutamate, as they cannot give up the proton and become charged. In these mutants the glutamate side chain either is absent (E148A) or does not bind to the pathway (E148Q), even when Cl^- is absent[43]. In contrast, in the WT protein the Glu148 side chain competes with the Cl^- ions for both S_{cen} and S_{ex}. This competition is likely to lower the affinity of Cl^- for those sites. In other words, in the WT protein the glutamate side chain acts as a tethered anion that competes with Cl^- and lowers its affinity. Thus, we propose that the high Cl^- affinity of the E148A and E148Q mutants arises from the lack of competition with the Glu148 side chain. This hypothesis offers a structural interpretation of the otherwise puzzling observation that these mutants have a high affinity for Cl^- even though their structures are nearly superimposable with that of the WT protein[31].

The observed 2:1 stoichiometry of Cl^--H^+ linked binding could arise through three scenarios: (i) Cl^- binding to both single-ion occupancy states (**Fig. 6d**,**e**) increases the protonation probability of Glu148 by ~50%; (ii) Cl^- binding to one of the single-ion occupancy states favors protonation of Glu148, whereas binding to the other state does not; (iii) our ITC experiments report on binding to a state with two Cl^- ions and one H^+ bound (**Fig. 6f**). Our data suggest that protonation of Glu148 is unfavorable with no ions in the transport pathway, favored by binding of a Cl^- ion to S_{cen} and greatly stabilized by a second Cl^- in S_{ex}. In contrast, protonation of the Glu148 side chain bound to S_{cen} remains unfavorable, regardless of whether S_{ex} is occupied by a Cl^- ion or not. Thus, we can rule out the first mechanism, as the two single-occupancy states have a very different impact on the protonation probability of Glu148. In contrast, our data suggest that both the second and third scenarios contribute to the measured 2:1 stoichiometry of linked binding. Finally, these results highlight the crucial role of Cl^- binding to S_{cen} in the coupling mechanism, consistent with previous experimental observations[38,42].

Relationship between coupled substrate binding and exchange

Our results have several implications for the transport mechanism of CLC-ec1 and, most probably, for all CLC transporters. One of the fundamental characteristics of the CLC exchangers is that they maintain a constant exchange stoichiometry of two Cl^- for one H^+, even though these proteins operate in a wide pH range (2–7) and have turnover rates ranging from 10 s^{-1} to nearly 10^5 s^{-1} (refs. 30,39). This characteristic is essential to allow these transporters to fulfill their physiological function: loss of H^+ coupling leads to disease-like phenotypes in mouse models[33]. Recently, it has been proposed that coupling in the CLCs is kinetic[29] rather than a result of the coordinated conformational changes of two gates, as it is in other transporters. In this model, the authors postulated that a high energy barrier slows down Cl^- movement between the central and internal binding sites so that, on average, two Cl^- ions transit per protonation or deprotonation event of Glu148. This argument, however, predicts that an acidic pH should degrade coupling, which is not observed in CLC-ec1 for pH values as low as 3 (refs. 22,41) or in CLC-5 at pH values as low as 5 (ref. 23). Furthermore, in CLC-ec1 and CLC-5 (ref. 32) the apparent pK_a of the external glutamate (Glu148 in CLC-ec1) is shifted by nearly two pH units, to ~6.2–6.5 (**Fig. 7**), so that its average protonated lifetime is ~10^{-4} s, assuming that the proton association rate is ~10^{10} M^{-1} s^{-1} (refs. 29,44). Thus, to prevent substantial slippage, the maximal transport rate of these proteins should be less than 10^2 s^{-1} (ref. 32), which is one-tenth to one-thousandth of their measured transport rates[30,39].

Our data offer an alternative, or complementary, mechanism to this kinetic model: that the 2:1 transport stoichiometry arises from the energetic requirement that two Cl^- ions bind to the transport pathway to lower the free energy barrier for protonation of Glu148. This coupling mechanism allows the stoichiometry of transport to remain constant in all CLC transporters, provided they share some basic characteristics, such as a glutamate at position 148, two conserved Cl^- binding sites and a network of hydrogen bonds that shield Glu148 from extra- and intracellular protons. Therefore, we propose that the stoichiometry of transport is hardwired into all CLC transporters by two conserved features: the energetic interactions between substrates bound to the protein and the structure of the CLC transport pathway. Our proposed mechanism also predicts and explains the observation that a reduction of anion binding affinity, through either mutagenesis[38] or substrate substitution[42,45], leads to degraded stoichiometry of binding and of transport. We speculate that the extremely degraded H^+/Cl^- coupling revealed by the irreversible gating of the CLC-0 channel[46,47] could result, at least in part, from the weakened Cl^- binding affinity of these proteins[48]. In other words, channels need to bind substrate weakly to sustain high rates of conduction, but this weak binding impairs the energetic coupling of Cl^- to protonation of the external glutamate.

We propose that the high free energy barrier that, in the absence of bound Cl^-, prevents protons from reaching the carboxyl side chain of Glu148, is a key mechanistic feature that allows CLC-ec1 to maintain coupling and presumably to preserve its proper function even at very low pH[22,41]. The absence of such a barrier would allow unhindered H^+ access to Glu148, leading to nearly permanent protonation of this residue in extreme acidic conditions, such as those found in the stomach[40]. This almost constitutive protonation would lead to a constitutively open Cl^- pathway, which would result in uncoupled Cl^- transport. In contrast, the tight regulation of the protonation probability of Glu148 by the Cl^- occupancy of the translocation pathway prevents this potentially lethal occurrence: protonation of Glu148 is permitted and stabilized by occupancy of the pathway by two Cl^- ions and is destabilized by Cl^- unbinding. Thus, during transport, binding of two Cl^- ions will induce protonation of Glu148, giving rise to a fully loaded protein state. Unbinding of Cl^- will destabilize the H^+ bound to Glu148, causing its deprotonation, thus promoting closure of the transport pathway and preventing uncoupling. It is possible that in some CLC transporters the free energy barrier that prevents protonation of the external glutamate when the pathway is

unoccupied by anions is lower than the one we found in CLC-ec1. This would allow these CLC transporters to become uncoupled when exposed to an acidic environment, as was recently documented for CLC-3 (ref. 49).

Our results suggest that in the CLC transporters, stoichiometric coupling of the substrates arises from the direct energetic interactions between the bound ions and the protein rather than, as previously proposed, from kinetic steps. Thus, in the CLC exchangers the stoichiometry of transport appears to be uniquely determined by the thermodynamics of synergistic substrate binding.

METHODS

Methods and any associated references are available in the online version of the paper at http://www.nature.com/nsmb/.

Note: Supplementary information is available on the Nature Structural & Molecular Biology website.

ACKNOWLEDGMENTS

The authors thank C. Miller (Brandeis University) for the gift of $^{36}Cl^-$ and D. Posson, D. Basilio, M. Malvezzi, C. Nimigean and H. Weinstein for helpful discussions and comments on the manuscript. This work was supported by grants from the National Institutes of Health (1R01GM085232 to A.A.) and by a grant from the Swiss National Science Foundation (SNF-Professorship #118928 to S.B.). Y.X. is supported by the China Scholarship Council. Part of the simulations were performed using the facilities of the Swiss National Supercomputing Centre (CSCS).

AUTHOR CONTRIBUTIONS

A.P. performed the ITC measurements; A.A. and A.P. performed the flux experiments and analyzed data; Y.X., N.J. and S.B. performed and analyzed the simulations; A.A. designed research and wrote the paper; all authors contributed to the editing of the manuscript.

COMPETING FINANCIAL INTERESTS

The authors declare no competing financial interests.

Published online at http://www.nature.com/nsmb/.
Reprints and permissions information is available online at http://www.nature.com/reprints/index.html.

1. Jardetzky, O. Simple allosteric model for membrane pumps. *Nature* **211**, 969–970 (1966).
2. Jennings, M.L. Structure and function of the red blood cell anion transport protein. *Annu. Rev. Biophys. Biophys. Chem.* **18**, 397–430 (1989).
3. Arkin, I.T. *et al.* Mechanism of Na^+/H^+ antiporting. *Science* **317**, 799–803 (2007).
4. Khare, D., Oldham, M.L., Orelle, C., Davidson, A.L. & Chen, J. Alternating access in maltose transporter mediated by rigid-body rotations. *Mol. Cell* **33**, 528–536 (2009).
5. Shimamura, T. *et al.* Molecular basis of alternating access membrane transport by the sodium-hydantoin transporter Mhp1. *Science* **328**, 470–473 (2010).
6. Kaback, H.R., Smirnova, I., Kasho, V., Nie, Y. & Zhou, Y. The alternating access transport mechanism in LacY. *J. Membr. Biol.* **239**, 85–93 (2011).
7. Radestock, S. & Forrest, L.R. The alternating-access mechanism of MFS transporters arises from inverted-topology repeats. *J. Mol. Biol.* **407**, 698–715 (2011).
8. Milanick, M.A. Ferret red cells: Na/Ca exchange and Na-K-Cl cotransport. *Comp. Biochem. Physiol. Comp. Physiol.* **102**, 619–624 (1992).
9. Sekler, I., Lo, R.S. & Kopito, R.R. A conserved glutamate is responsible for ion selectivity and pH dependence of the mammalian anion exchangers AE1 and AE2. *J. Biol. Chem.* **270**, 28751–28758 (1995).
10. Beaugé, L. & DiPolo, R. The squid axon Na^+/Ca^{2+} exchanger shows ping-pong kinetics only when the Cai-regulatory site is saturated. *Cell. Physiol. Biochem.* **23**, 37–42 (2009).
11. Adam, Y., Tayer, N., Rotem, D., Schreiber, G. & Schuldiner, S. The fast release of sticky protons: kinetics of substrate binding and proton release in a multidrug transporter. *Proc. Natl. Acad. Sci. USA* **104**, 17989–17994 (2007).
12. Restrepo, D., Cronise, B.L., Snyder, R.B. & Knauf, P.A. A novel method to differentiate between ping-pong and simultaneous exchange kinetics and its application to the anion exchanger of the HL60 cell. *J. Gen. Physiol.* **100**, 825–846 (1992).
13. Contreras-Jurado, C., Sanchez-Morito, N., Ruiz-Contreras, A., Gonzalez-Martinez, M.T. & Soler-Diaz, A. Evidence for simultaneous $1Na^+$:$1Mg^{2+}$ and ping-pong $2Na^+$:$1Mg^{2+}$ exchangers in rat thymocyte. *Front. Biosci.* **10**, 1693–1706 (2005).
14. Dutzler, R., Campbell, E.B., Cadene, M., Chait, B.T. & MacKinnon, R. X-ray structure of a ClC chloride channel at 3.0 Å reveals the molecular basis of anion selectivity. *Nature* **415**, 287–294 (2002).
15. Abramson, J. *et al.* Structure and mechanism of the lactose permease of *Escherichia coli*. *Science* **301**, 610–615 (2003).
16. Yernool, D., Boudker, O., Jin, Y. & Gouaux, E. Structure of a glutamate transporter homolog from *Pyrococcus horikoshii*. *Nature* **431**, 811–818 (2004).
17. Yamashita, A., Singh, S.K., Kawate, T., Jin, Y. & Gouaux, E. Crystal structure of a bacterial homolog of Na^+/Cl^--dependent neurotransmitter transporters. *Nature* **437**, 215–223 (2005).
18. Morth, J.P. *et al.* Crystal structure of the sodium-potassium pump. *Nature* **450**, 1043–1049 (2007).
19. Olesen, C. *et al.* The structural basis of calcium transport by the calcium pump. *Nature* **450**, 1036–1042 (2007).
20. Fang, Y. *et al.* Structure of a prokaryotic virtual proton pump at 3.2-Å resolution. *Nature* **460**, 1040–1043 (2009).
21. Shaffer, P.L., Goehring, A., Shankaranarayanan, A. & Gouaux, E. Structure and mechanism of a Na^+-independent amino acid transporter. *Science* **325**, 1010–1014 (2009).
22. Accardi, A. & Miller, C. Secondary active transport mediated by a prokaryotic homolog of ClC Cl^- channels. *Nature* **427**, 803–807 (2004).
23. Scheel, O., Zdebik, A.A., Lourdel, S. & Jentsch, T.J. Voltage-dependent electrogenic chloride/proton exchange by endosomal CLC proteins. *Nature* **436**, 424–427 (2005).
24. Picollo, A. & Pusch, M. Chloride/proton antiporter activity of mammalian CLC proteins ClC-4 and ClC-5. *Nature* **436**, 420–423 (2005).
25. De Angeli, A. *et al.* The nitrate/proton antiporter AtCLCa mediates nitrate accumulation in plant vacuoles. *Nature* **442**, 939–942 (2006).
26. Graves, A.R., Curran, P., Smith, C. & Mindell, J. The Cl^-/H^+ antiporter ClC-7 is the primary chloride permeation pathway in lysosomes. *Nature* **453**, 788 (2008).
27. Matsuda, J.J. *et al.* Overexpression of CLC-3 in HEK293T cells yields novel currents that are pH dependent. *Am. J. Physiol. Cell Physiol.* **294**, C251–262 (2008).
28. Accardi, A. *et al.* Separate ion pathways in a Cl^-/H^+ exchanger. *J. Gen. Physiol.* **126**, 563–570 (2005).
29. Feng, L., Campbell, E.B., Hsiung, Y. & MacKinnon, R. Structure of a eukaryotic CLC transporter defines an intermediate state in the transport cycle. *Science* **330**, 635–641 (2010).
30. Zdebik, A.A. *et al.* Determinants of anion-proton coupling in mammalian endosomal CLC proteins. *J. Biol. Chem.* **283**, 4219–4227 (2008).
31. Dutzler, R., Campbell, E.B. & MacKinnon, R. Gating the selectivity filter in ClC chloride channels. *Science* **300**, 108–112 (2003).
32. Accardi, A. & Picollo, A. CLC channels and transporters: proteins with borderline personalities. *Biochim. Biophys. Acta* **1798**, 1457–1464 (2010).
33. Novarino, G., Weinert, S., Rickheit, G. & Jentsch, T.J. Endosomal chloride-proton exchange rather than chloride conductance is crucial for renal endocytosis. *Science* **328**, 1398–1401 (2010).
34. Baker, B.M. & Murphy, K.P. Evaluation of linked protonation effects in protein binding reactions using isothermal titration calorimetry. *Biophys. J.* **71**, 2049–2055 (1996).
35. Petrosian, S.A. & Makhatadze, G.I. Contribution of proton linkage to the thermodynamic stability of the major cold-shock protein of *Escherichia coli* CspA. *Protein Sci.* **9**, 387–394 (2000).
36. Velazquez-Campoy, A. *et al.* Thermodynamic dissection of the binding energetics of KNI-272, a potent HIV-1 protease inhibitor. *Protein Sci.* **9**, 1801–1809 (2000).
37. Picollo, A., Malvezzi, M., Houtman, J. & Accardi, A. Basis of substrate binding and conservation of selectivity in the CLC family of channels and transporters. *Nat. Struct. Mol. Biol.* **16**, 1294–1301 (2009).
38. Accardi, A., Lobet, S., Williams, C., Miller, C. & Dutzler, R. Synergism between halide binding and proton transport in a CLC-type exchanger. *J. Mol. Biol.* **362**, 691–699 (2006).
39. Walden, M. *et al.* Uncoupling and turnover in a Cl^-/H^+ exchange transporter. *J. Gen. Physiol.* **129**, 317–329 (2007).
40. Iyer, R., Iverson, T.M., Accardi, A. & Miller, C. A biological role for prokaryotic ClC chloride channels. *Nature* **419**, 715–718 (2002).
41. Accardi, A., Kolmakova-Partensky, L., Williams, C. & Miller, C. Ionic currents mediated by a prokaryotic homolog of CLC Cl^- channels. *J. Gen. Physiol.* **123**, 109–119 (2004).
42. Nguitragool, W. & Miller, C. Uncoupling of a CLC Cl^-/H^+ exchange transporter by polyatomic anions. *J. Mol. Biol.* **362**, 682–690 (2006).
43. Lobet, S. & Dutzler, R. Ion-binding properties of the ClC chloride selectivity filter. *EMBO J.* **25**, 24–33 (2006).
44. Jenks, W.P. *Catalysis in Chemistry and Enzymology*. (McGraw Hill Text, 1969).
45. Zifarelli, G. & Pusch, M. Conversion of the 2 Cl^-/1 H^+ antiporter ClC-5 in a NO_3^-/H^+ antiporter by a single point mutation. *EMBO J.* **28**, 175–182 (2009).
46. Richard, E.A. & Miller, C. Steady-state coupling of ion-channel conformations to a transmembrane ion gradient. *Science* **247**, 1208–1210 (1990).
47. Lísal, J. & Maduke, M. The ClC-0 chloride channel is a 'broken' Cl^-/H^+ antiporter. *Nat. Struct. Mol. Biol.* **15**, 805–810 (2008).
48. Chen, M.F. & Chen, T.Y. Side-chain charge effects and conductance determinants in the pore of ClC-0 chloride channels. *J. Gen. Physiol.* **122**, 133–145 (2003).
49. Matsuda, J.J., Filali, M., Collins, M., Volk, K. & Lamb, F. The ClC-3 Cl^-/H^+ antiporter becomes uncoupled at low extracellular pH. *J. Biol. Chem.* **285**, 2569–2579 (2010).

ONLINE METHODS

Protein purification. Expression and purification of CLC-ec1 was performed according to published protocols[28,38,41]. The protein was run on a Superdex 200 column (GE Healthcare) pre-equilibrated in 100 mM Na-K-tartrate, 5 mM *n*-decyl-β-D-maltoside (DM) and 20 mM Tris (buffer R_T), HEPES (buffer R_H) or phosphate–H_2SO_4 (buffer R_P), pH 7.5. Salts and buffers were purchased from Sigma and DM was purchased from Anatrace.

Binding measurements with isothermal titration calorimetry. ITC measurements were performed using either a VP-ITC or an ITC200 Titration Calorimeter (Microcal, Inc.) or a Nano ITC (TA Instruments). The thermodynamic parameters of binding measured with the three machines were comparable in all tested cases. Protein was concentrated to 80–180 μM and added to the experimental chamber. The injection syringe was filled with the appropriate buffer (R_T, R_H or R_P), to which 5–100 mM of KCl was added based on the desired final molar ratio of injectant to CLC-ec1. Each experiment consisted of 20–35 injections into the experimental chamber of 1–10 μl of the ligand solution at 3–4 min intervals. The experimental chamber was kept under constant stirring at 350 r.p.m. at 25.0 ± 0.1 °C. All solutions were filtered and degassed before use. The protein was extensively dialyzed between runs and re-used.

Fitting ITC data. Fits were performed using the same procedure as described[37]. Briefly, the dilution heats of the protein and of the salt were determined independently and subtracted from each experiment. The data were fit to the Wiseman isotherm using the Origin ITC analysis package or the NanoAnalyze program from TA Instruments. The different shapes of the ITC curves are due to the different affinities of Cl^- for WT and mutant CLC-ec1 variants[37]. The general shape of an ITC curve is determined by the value of the product of the association constant and the receptor concentration, called the *c* value[50]. When $c > 5$, the curve takes a characteristic sigmoid shape; when $c < 5$, the curve becomes progressively more hyperbolic. For WT CLC-ec1 and the E203Q and Y445L mutants, $c < 1$, so the curves are hyperbolic. In contrast, the E148A mutant has a higher affinity for Cl^-, so that $c \sim 9$ and the curve is sigmoidal. The enthalpy of ionization of the various buffers, ΔH_{buff}, was determined experimentally (**Supplementary Table 1**) following established protocols[51].

Cl^- uptake measurements. Measurements were carried out as previously described[41,52]. Individual uptake time courses were fitted to a saturating single exponential function of the form $C(t) = a_M \times (1-\exp(-t/\tau)$, where $C(t)$ represents the fractional counts at time t, a_M is the maximum fraction of radioactivity trapped, t is time and τ is the time constant of uptake. Individual time courses were normalized to a_M to yield the normalized uptake and averaged among different experiments. In some cases the time course of uptake was very slow and a fit with an exponential was inappropriate. In these cases we fit the data to $C(t) = a_M \times t/\tau$ and a_M was kept fixed to the averaged value measured at pH values at which saturation could be reached, as the trapped volume does not depend on the pH of reconstitution[41].

Mutagenesis. All mutagenesis was carried out with the QuikChange method (Stratagene) and the mutated genes fully sequenced.

Free energy calculations. The molecular systems used for the calculations were assembled using the CHARMM-GUI web service[53]. All systems comprise the ClC-ec1 dimer (PDB: 1OTS[31]) embedded in a bilayer composed of 242 dimystoylphosphatidylcholine (DMPC) lipid molecules and solvated by a ~150-mM KCl solution. The systems were equilibrated according to the different protonation and ion occupancy states listed in **Supplementary Table 2**. In the two-ion state (**Fig. 6f**), both the central (S_{cen}) and external (S_{ext}) binding sites are occupied by Cl^-, whereas in the single-ion states (**Fig. 6d**,**e**), S_{cen} and S_{ex} are alternatively occupied by an ion. No restraint was applied to the glutamate residues during equilibration. The side chain of Glu148 spontaneously moves from S_{ext} to S_{cen} when no Cl^- is present in the pore (**Fig. 6c**). An *N*-acetyl-Glu-(*N*′)-methylamide dipeptide was placed in solution, away from the membrane, and serves as a proton donor or acceptor. The reported free energy differences thus correspond to the work done to transfer a proton between this solvated dipeptide and a glutamate residue in the protein. Two different protocols (A and B) were used for the staged free energy perturbation calculations: protocol A, $\Delta\lambda$ of 0.1, 11 windows, 20 ps per window, including 2 ps of equilibration; protocol B, $\Delta\lambda$ of 0.05, 21 windows, 50 ps per window, including 10 ps of equilibration, where λ is a scaling factor from 0 to 1 which represents the state of the system. In the calculations for the protonation reaction, $\lambda = 0$ corresponds to the state where the proton is on the solvated dipeptide and $\lambda = 1$ corresponds to the state in which the glutamate in the protein is protonated. In the calculations for the deprotonation reaction, the states are exchanged. Simulations were performed using the PERT module of the CHARMM software[54] with the PARAM27 force field[55]. All simulation parameters were as described elsewhere for other membrane systems[56]. The free energy difference between the end states was obtained by combining sampling from forward and backward simulations using the WHAM module[57] of CHARMM, which is in all point equivalent to the more recently popularized multistate Bennett acceptance ratio (MBAR) approach[58]. According to the MBAR analysis, the forward and backward perturbations are not required to give the same results for the final calculated free energy difference to be reliable. They are complementary in providing information on different portion of the configuration space[59]. The forward and backward results are nevertheless reported in **Supplementary Table 2**, as they provide further information on the stability of the end states.

Unless otherwise stated, we used for the protonatable residues their natural protonation state at pH 7, which is a value close to that used in the ITC experiments. This assumption is consistent with previous work[60] that showed that only Glu148, Glu113 and Glu203 have severely shifted pK_a values. It is worth noting that protonation of Glu203 when Glu113 is already protonated sometime leads to diverging results. In general, when Glu113 is protonated, the two residues form a hydrogen bond, which impedes the protonation of Glu203. However, the two residues can occasionally be linked by one or more water molecules. In such case, protonation of Glu203 can be favorable. These alternative conformations are possibly relevant to the proton permeation mechanism and will require further investigations.

Data analysis and figure preparation. Flux data was analyzed using the Ana (http://www.ge.ibf.cnr.it/~pusch.ibf/programs-mik.htm) and SigmaPlot (Systat Software, Inc.) softwares. Molecular models were prepared using Pymol (Open-Source PyMOL 0.99rc6) and VMD (v1.9, http://www.ks.uiuc.edu/Research/vmd/).

50. Thomson, J.A. & Ladbury, J.E. in *Biocalorimetry 2: Applications of Calorimetry in the Biological Sciences* (eds. Ladbury, J.E. & Doyle, M.L.) Ch. 2 (Wiley, 2004).
51. Fukada, H. & Takahashi, K. Enthalpy and heat capacity changes for the proton dissociation of various buffer components in 0.1 M potassium chloride. *Proteins* **33**, 159–166 (1998).
52. Maduke, M., Pheasant, D.J. & Miller, C. High-level expression, functional reconstitution, and quaternary structure of a prokaryotic ClC-type chloride channel. *J. Gen. Physiol.* **114**, 713–722 (1999).
53. Jo, S., Kim, T., Iyer, V.G. & Im, W. CHARMM-GUI: a web-based graphical user interface for CHARMM. *J. Comput. Chem.* **29**, 1859–1865 (2008).
54. Brooks, B.R. *et al.* CHARMM: the biomolecular simulation program. *J. Comput. Chem.* **30**, 1545–1614 (2009).
55. MacKerell, A.D. Jr. *et al.* All-atom empirical potential for molecular modeling and dynamics studies of proteins. *J. Phys. Chem. B* **102**, 3586–3616 (1998).
56. Boiteux, C. & Bernèche, S. Absence of ion-binding affinity in the putatively inactivated low-[K^+] structure of the KcsA potassium channel. *Structure* **19**, 70–79 (2011).
57. Souaille, M. & Roux, B. Extension to the weighted histogram analysis method: combining umbrella sampling with free energy calculations. *Comput. Phys. Commun.* **135**, 40–57 (2001).
58. Shirts, M.R. & Chodera, J.D. Statistically optimal analysis of samples from multiple equilibrium states. *J. Chem. Phys.* **129**, 124105 (2008).
59. Pohorille, A., Jarzynski, C. & Chipot, C. Good practices in free-energy calculations. *J. Phys. Chem. B* **114**, 10235–10253 (2010).
60. Faraldo-Gómez, J.D. & Roux, B. Electrostatics of ion stabilization in a ClC chloride channel homolog from *Escherichia coli*. *J. Mol. Biol.* **339**, 981–1000 (2004).

doi:10.1038/nsmb.2277